Ice surface changes along the Jutulstraumen and Penck Trough ice streams in western Dronning Maud Land, East Antarctica, during recent glacial cycles

J.L. Andersen[1,2*], J.C. Newall[1,3,4], R. Blomdin[3,4], S.E. Sams[1], D. Fabel[5], A.J. Koester[1], N.A. Lifton[1,6], O. Fredin[2,7], M.W. Caffee[1,6], Neil F. Glasser[8], I. Rogozhina[7], Y. Suganuma[9,10], J.M. Harbor[1,3,4,11], A.P. Stroeven[3,4]

[1]Department of Earth, Atmospheric, and Planetary Sciences, Purdue University, West Lafayette, USA

[2]Geological Survey of Norway, Trondheim, Norway

[3]Geomorphology & Glaciology, Department of Physical Geography, Stockholm University, Stockholm, Sweden

[4]Bolin Centre for Climate Research, Stockholm University, Stockholm, Sweden

[5]Scottish Universities Environmental Research Centre, Glasgow, UK

[6]Department of Physics and Astronomy, Purdue University, West Lafayette, USA

[7]Department of Geography, Norwegian University of Science and Technology, Trondheim, Norway

[8]Centre for Glaciology, Department of Geography and Earth Sciences, Aberystwyth University, Aberystwyth, UK

[9]National Institute of Polar Research, Japan

[10]The Graduate University for Advanced Studies, SOKENDAI, Japan

[11]Departments of Geography and Geosciences, University of Montana, Missoula, USA

[*]Correspondence to: jane.lund@geo.au.dk, Present address: Department of Geoscience, Aarhus University, Denmark

Keywords: Antarctica; Glaciation; Quaternary; Cosmogenic isotopes; Dronning Maud Land

Abstract

Reconstructing past ice-sheet surface changes is key to test and improve ice-sheet models. Data constraining the past behaviour of the East Antarctic Ice Sheet are sparse, limiting our understanding of its response to past, present and future climate change. Here, we report the first cosmogenic multi-nuclide (^{10}Be, ^{26}Al, ^{36}Cl) data from bedrock and erratics on nunataks along the Jutulstraumen and Penck Trough ice streams in western Dronning Maud Land, East Antarctica. Spanning elevations between 751 and 2387 m above sea level, the samples record apparent exposure ages between 2 ka and 5 Ma. The highest-elevation bedrock sample indicates (near-) continuous minimum exposure since the Pliocene, with a low apparent erosion rate of 0.15±0.03 m Ma^{-1}, similar to results from eastern Dronning Maud Land. In contrast to studies in eastern Dronning Maud Land, there are clear indications of a thicker-than-present ice sheet within the last glacial cycle, with a thinning of ~35–120 m towards the present ice surface on several nunataks during the Holocene (~2– 11 ka). Owing to difficulties in retrieving suitable sample material from the often rugged and quartz-poor mountains, and because of inherited nuclides in many of our samples, we are unable to present robust thinning estimates from elevational profiles. Nevertheless, the results clearly indicate ice-surface fluctuations of several hundred meters between the current grounding line and the edge of the polar plateau for the last glacial cycle, a constraint that should be considered in future ice-sheet model simulations.

1. Introduction

Constraining the sensitivity of the East Antarctic Ice Sheet (EAIS) to climate changes is an important challenge to the scientific community, as even modest variations in this vast ice mass impacts global sea level and climate dynamics (DeConto and Pollard, 2016; Mengel et al., 2018). Delineating EAIS configuration changes during the last glacial cycle will help minimize uncertainties in estimates of ongoing glacial isostatic adjustment that obscures present-day mass balance budgets derived from satellite gravimetry (Velicogna and Wahr, 2006, 2013; Riva et al., 2009; Thomas et al., 2011). Yet, observational constraints on past EAIS volume variations and dynamics are scarce owing to a combination of remote and harsh working conditions, and a lack of materials readily available for dating because 98% of the Antarctic continent is covered by ice.

First order changes in the large-scale configuration of the EAIS during the last glacial cycle have been reconstructed using ice-core and marine records. While ice-core records indicate that interior domes thinned by 110–120 m in response to climate cooling towards the Last Glacial Maximum (LGM, ~27–20 ka; Parrenin et al., 2007), marine records show that ocean-terminating margins concurrently advanced to the continental shelf break along most sectors (Bentley et al., 2014). The pattern of thinner, yet more extensive ice, indicates that colder ocean temperatures and more extensive sea-ice cover may have reduced inland precipitation and thereby thinning the interior parts of the ice sheet during glacial periods (Suganuma et al., 2014; Yamane et al., 2015), while simultaneously allowing ice-sheet margins to advance in most areas under the influence of global sea level fall. Scattered marine and terrestrial records point to a large variability in the response of various East Antarctic sectors during the last glacial cycle. These records show that several East Antarctic sectors (e.g. Bunger Hills, Larsemann Hills, Sôya coast in Lützow-Holm Bay) experienced only limited ice-sheet margin advances during the LGM (Fig. 2; Miura et al., 1998; Gore et al., 2001; Hodgson et al., 2001; Mackintosh et al., 2014) and that the timing of post-LGM ice-sheet recession varies markedly between individual sectors, with ice receding as early as 18 ka in some areas (Lambert-Amery glacial system) but much later in other areas (e.g. Bunger Hills, Lützow-Holm Bay, Framnes mountains) where the main ice recession occurred during the Early- to Mid-Holocene (Mackintosh et al., 2014).

Cosmogenic nuclide exposure dating of coastal islands and nunataks protruding through the ice sheet in coastal, mountainous areas are key to constraining the timing of ice-sheet retreat and thinning, and thus marginal ice-sheet surface gradients and volume changes of the ice sheet. To improve our understanding of the response of coastal sectors of the EAIS to past climate changes, it is critical to increase the density of well-dated records by filling the data gaps around the EAIS. One such data gap exists in western Dronning Maud Land, where few chronological constraints of past EAIS behaviour exist (Fig. 1). In this study, we combine ^{10}Be ($t_{1/2}$=1.39 Myr; Chmeleff et al., 2010; Korschinek et al., 2010), ^{26}Al ($t_{1/2}$=0.705 Myr; Nishiizumi, 2004), and ^{36}Cl ($t_{1/2}$=0.301 Myr; Holden, 1990) measurements in bedrock and erratic samples from nunataks protruding through the EAIS along the Jutulstraumen and Penck Trough ice streams in western Dronning Maud Land, East Antarctica (~0–4ºW, 71.5–73ºS), in an effort to understand how the ice sheet responded to climate changes during recent glacial cycles.

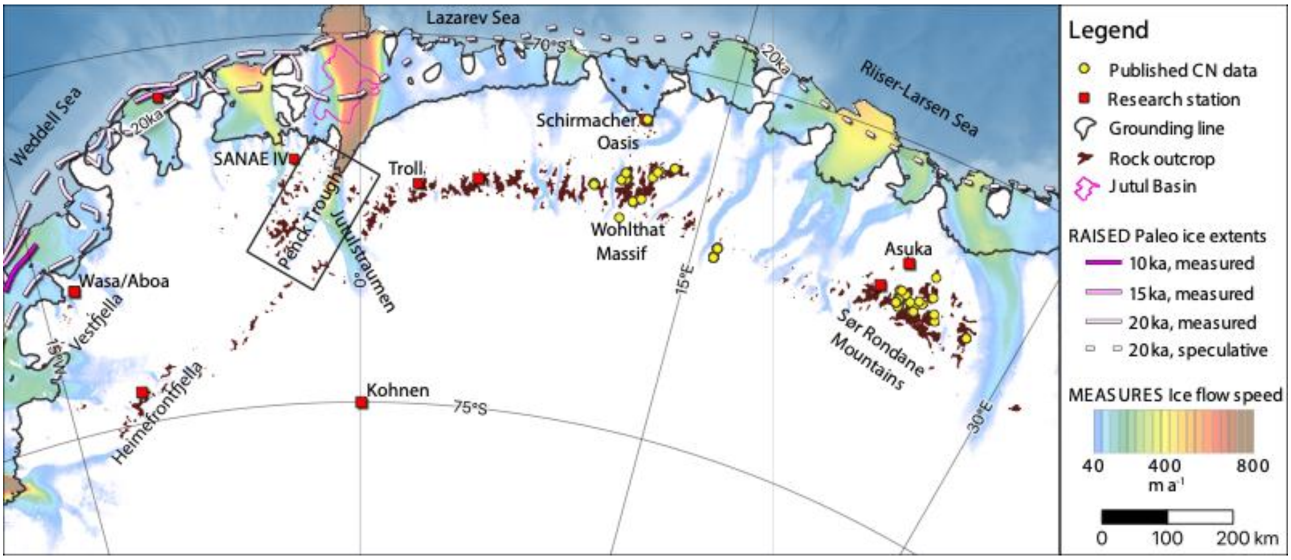

Fig. 1. *Overview map of Dronning Maud Land with published cosmogenic nuclide (CN) data and localities mentioned in text. The black rectangle outlines the study area. RAISED Paleo-ice extents by Bentley et al. (2014), and MEASURES present-day ice flow speed by Rignot et al. (2017). The Jutul Basin is outlined in pink with the 600 m contour of water depth below the Fimbulisen Ice Shelf, derived from Fretwell et al. (2013). Published cosmogenic nuclide data are from Heyman (http://expage.github.io, accessed 20.02.20), all other data acquired through the Quantarctica package (Matsuoka et al., 2018).*

2. Study Area

Dronning Maud Land is considered to be one of the main nucleation points of the EAIS when it formed in the Late Eocene, and ice-sheet models indicate a continuous but variable presence of ice in this region since then (DeConto and Pollard, 2003). The Dronning Maud Land margin is characterised by a 1500 km long and up to 3 km a.s.l. (above sea level) high escarpment stretching along parts of the Atlantic and Indian sectors of the Southern Ocean (Fig. 1; Fretwell et al., 2013). The escarpment obstructs ice flow from the inland polar plateau (Rignot et al., 2011, 2017), while simultaneously acting as a barrier for moisture transport from the Southern Ocean leading to a sharp inland decrease in precipitation from 0.2–0.7 m a^{-1} (ice equivalents) in the coastal region to <0.1 m a^{-1} above the escarpment (Arthern et al., 2006; van de Berg et al., 2006). Only a few topographic troughs dissect the escarpment in Dronning Maud Land, facilitating ice flow from the higher polar plateau to the lower coastal part of the EAIS (Fig. 1). The most prominent of these troughs, up to 50 km wide and more than 1.6 km below present sea level (Fretwell et al., 2013), contains the Jutulstraumen ice stream, which drains the EAIS with velocities up to 760 m a^{-1} at the grounding line (Fig. 1; Rignot et al., 2017). As Jutulstraumen enters the structurally-controlled Penck Trough within our study area, it makes a ~60° turn changing from a NW to a NE direction of ice flow (Figs. 1, 2). Beyond the present-day grounding line, the trough extends into the 'Jutul Basin', covered by the Fimbulisen Ice Shelf which is ~100–200 km wide and extends close to the continental shelf break (Fig. 1; Smedsrud et al., 2006; Fretwell et al., 2013). The maximum water depth below Fimbulisen exceeds 800 m in the Jutul Basin, whereas zones of grounded ice flank the trough on both its sides, and the Jutul Sill at ~70° S limits water depths to ~300 m towards the Southern Ocean (Smedsrud et al., 2006; Fretwell et al., 2013). In an inland direction, the NE–SW-striking Penck Trough becomes approximately tangential to the escarpment ~270 km from the grounding line, whereas the nearest part of the escarpment is only ~100 km from the grounding line in a S-SE direction (Fig. 2).

Mean annual surface air temperatures are -30 to -14 °C within our study area on the coastal ice below the escarpment (1979-1998; Comiso, 2000), while the temperature increase in Dronning Maud Land observed at the Kohnen Station (Fig. 1, 75°S, 0.04°E, 2892 m a.s.l.) above the escarpment is outpacing any other East Antarctic regions with instrumental records (1.15±0.71 °C decade^{-1} since 1997; Medley et al., 2018). Meanwhile, satellite records indicate that the ice surface in Dronning Maud Land has thickened by up to a decimetre per year over the last 25 years (Schröder et al., 2019), although this estimate is strongly influenced by large snowfall events in 2009 and 2011 (Lenaerts et al., 2013). If snow accumulation continues to increase at these rates, it is possible that Dronning Maud Land snowfall could mitigate sea-level contributions from ice loss in West Antarctica and the Antarctic Peninsula (Medley et al., 2018).

Estimates of the ice-sheet extent offshore from Dronning Maud Land during the LGM remain speculative (Anderson et al., 2002; Livingstone et al., 2012; Bentley et al., 2014), although scattered sedimentological and radiocarbon data indicate ice-sheet advance to the continental shelf break towards the eastern Weddell Sea sector around 21 ka (Fig. 1; Elverhøi 1981; Anderson et al., 2002; Bentley et al., 2014).

In eastern Dronning Maud Land, cosmogenic nuclide exposure data indicate long-term lowering of the ice-sheet surface since the Pliocene, and limited ice-sheet thickening during the LGM. Studies from the Sør Rondane Mountains (Fig. 1) constrain ice thickening during the LGM to <100 m for samples 65–135 km inland from the present-day ice-sheet margin (Matsuoka et al., 2006; Suganuma et al., 2014; Yamane et al., 2015), whereas data from the Wohlthat Massif (Fig. 1) indicate <50 m thickening during the LGM, 80–160 km inland from the present ice-sheet margin (Altmaier et al., 2010; Strub et al., 2015). Surface exposure data adjacent to the present grounding line in Schirmacher Oasis (Fig. 1) indicate thicker ice during the LGM, although the magnitude of ice thickening is uncertain since the oasis is nearly flush with the present-day ice surface (Altmaier et al., 2010). There is a paucity of cosmogenic nuclide exposure data in western Dronning Maud Land. However, observations of spatially uniform glacial striation directions and of relatively unweathered lodgement-till deposits in the Vestfjella and Heimefrontfjella mountains (Fig. 1) indicate that the EAIS was thicker than today with magnitude of ice-sheet thickening increasing from <50 m in the area around Scharffenbergbotnen in Heimefrontfjella (ca. 130 km inland from the present-day grounding line; Lintinen and Nenonen, 1997; Hättestrand and Johansen, 2005), to >700 m above present ice surface at the coastal nunatak Plogen, Vestfjella (Lintinen 1996; Lintinen and Nenonen, 1997). Radiocarbon dates on the basal layers of regurgitated stomach oil deposits (mumiyo) from snow petrel (*Pagodroma nivea*) nesting sites indicate ice-free conditions since at least 0.7–7.8 cal ka BP (reported conventional radiocarbon ages: 2.1–8.2 ka; Lintinen and Nenonen, 1997) at nesting sites 100–230 m above the present ice surface at Skuafjellet in Vestfjella, while sites 30–200 m above the ice in Scharffenbergbotnen were ice free from at least 4.2–8.3 cal ka BP (reported conventional radiocarbon ages: 4.9–8.7 ka; Lintinen and Nenonen, 1997). We calibrated these ages using CALIB REV7.1.0 with the Southern Hemisphere calibration (Stuiver and Reimer 1993; Hogg et al., 2013), and deducted an Antarctic marine reservoir effect of ~1.3 ka (Steele and Hiller, 1997). The ages are similar to those of basal mumiyo from snow petrel nesting sites near the Penck Trough and the Troll research station (Figs. 1, 2), which indicate ice free conditions 1–100 m above present ice level since 1.4-8.0 cal ka BP (reported conventional radiocarbon ages corrected for 1.3 ka marine reservoir effect: 0.8–7.0 ka; Steele and Hiller, 1997).

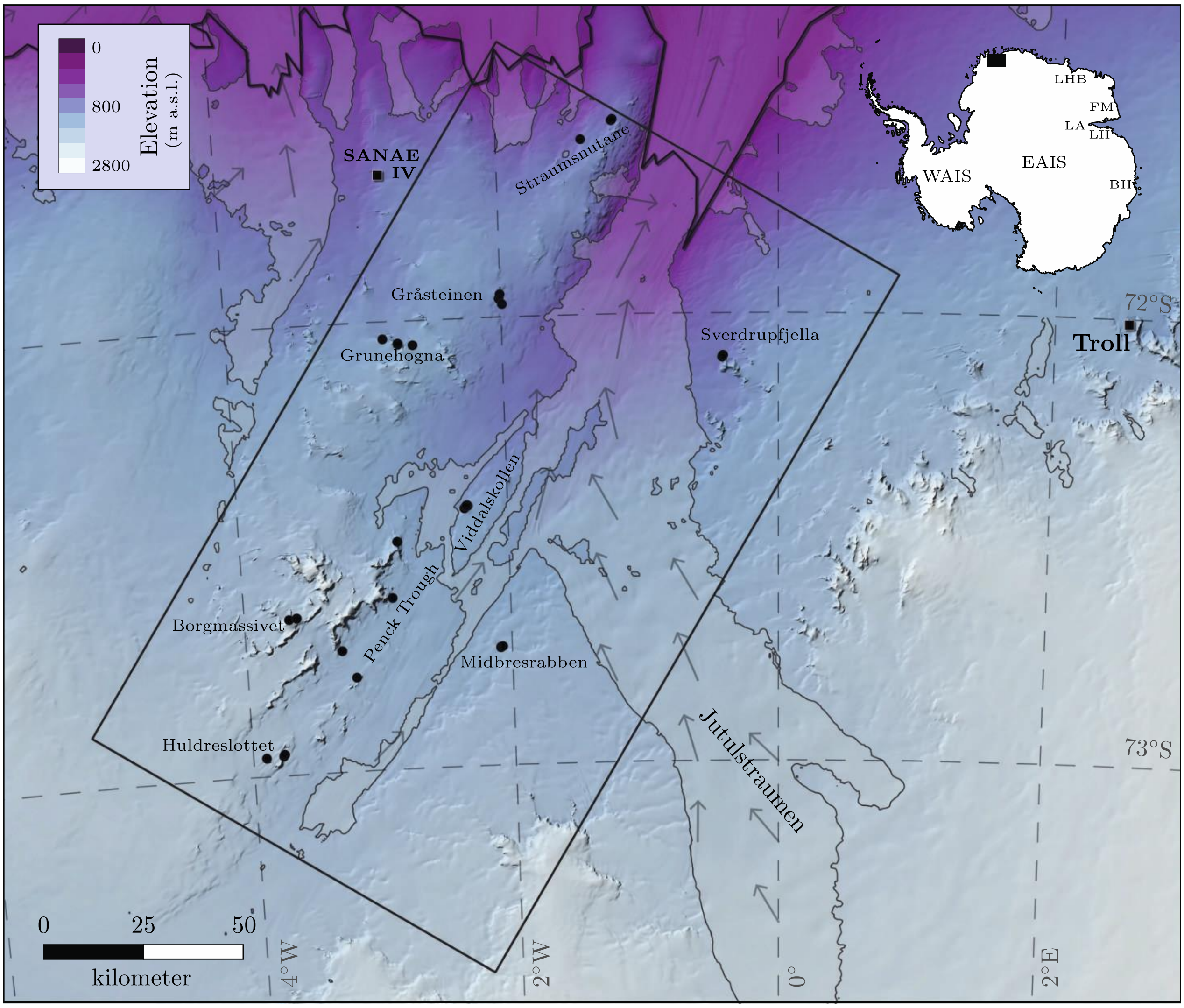

Fig. 2. *Sample site locations along the Penck Trough. Inset indicates the extent of the map in Antarctica (filled black rectangle), with place names mentioned in text: WAIS=West Antarctic Ice Sheet, EAIS=East Antarctic Ice Sheet, LHB: Lützow-Holm Bay, FM: Framnes Mountains, LA: Lambert-Amery glacial system, LH: Larsemann Hills, BH: Bunger Hills. On the main map, Troll (Norwegian) and Sanae (South African) research stations are marked for orientation. Sample sites are marked with black dots and nunatak name. Note that the 'Penck Trough Assemblage' consists of four single samples collected from four nunataks all proximal to the Penck Trough. The grounding line is traced in black, and areas where current ice flow exceeds 40 m a^{-1} are outlined in black with transparent white fill, arrows within these regions indicate direction and magnitude of present-day ice flow (Rignot et al., 2017). The black rectangle outlines the area used for the swath profile shown in Fig. 5. Topographic data are sourced from REMA (Howat et al., 2019), all other data acquired through the Quantarctica 3 package (Matsuoka et al., 2018).*

3. Methods

3.1. Cosmogenic nuclide exposure dating

Cosmogenic nuclides accumulate *in situ* in bedrock and surficial debris near the surface of the Earth as a result of nuclear changes induced by high-energy particles from space (Gosse and Phillips, 2001). Cosmogenic nuclide exposure dating is commonly applied to glacial deposits and landforms. By employing nuclide-specific and temporally- and spatially- varying production rates, the inventory of cosmogenic nuclides measured in a rock surface can be converted into an apparent exposure age. The short attenuation length of the dominant spallation reaction (~150–230 g cm^{-2}; Marrero et al., 2016) results in measurable nuclide inventories mainly within the upper 3 m of bedrock. This means that a few meters of bedrock erosion can reduce surficial nuclide inventories to below analytical precision. If sufficient erosion takes place during a period of glacial cover to erode nuclides from prior exposure, an apparent exposure age of a sample then reflects the time since last deglaciation, in the absence of subsequent subaerial erosion or burial. However, the hyper-arid polar climate of East Antarctica leads to cold-based conditions beneath much of the ice sheet outside of major troughs (Näslund et al., 2000; Altmaier et al., 2010). Both Northern (e.g. Stroeven et al., 2002; Briner et al., 2014) and Southern (e.g. Nichols et al., 2019) Hemisphere studies demonstrate the inability of cold-based ice to erode sufficient material to remove nuclide inventories. This frequently leads to apparent exposure ages that overestimate the timing of last deglaciation, reflecting a complex history of exposure and burial (e.g., Stroeven et al., 2016). To distinguish between simple and complex exposure histories, multiple nuclides with different half-lives can be analysed (Gosse and Phillips, 2001; Altmaier et al., 2010); a strategy we employ in this study.

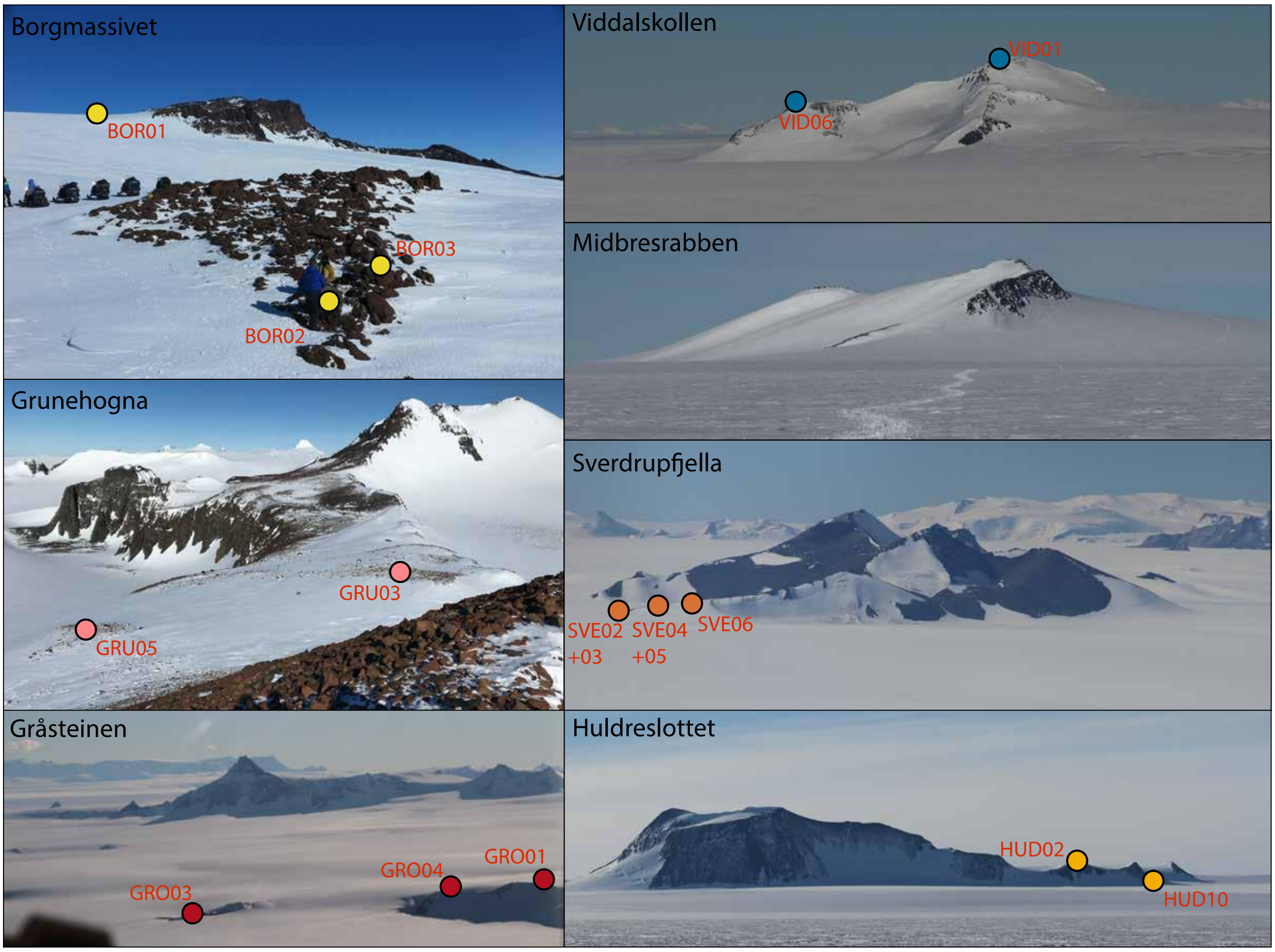

Fig. 3. *Photographs of sample sites with location of samples within view indicated by coloured circles. The fill colours for each site is maintained in the following figures. No good overview photos were obtained from the Penck Trough Assemblage or Straumsnutane sample sites. All samples from Midbresrabben and non-labelled samples from Viddalskollen were collected on the far side of the nunataks. One additional sample from Huldreslottet, and two samples from Grunehogna were collected at other nunataks in the area and are not shown.*

3.2. Sampling campaign and sample selection criteria

We collected and analysed samples from bedrock (n=20) and erratics (n=15) on nunataks flanking a 190 km-long transect of the Penck Trough and Jutulstraumen ice streams in western Dronning Maud Land (Fig. 2), with the aim of constructing a series of elevation profiles between the escarpment and the present-day ice margin. Samples were collected using a battery-powered impact drill, hammer, and wedges in January 2018 on the following nunataks (listed in order of increasing distance from the grounding line): Straumsnutane (n=4), Sverdrupfjella (n=5), Gråsteinen (n=3), Grunehogna (n=4), Viddalskollen (n=5), Midbresrabben (n=4), Penck Trough Assemblage (our name; n=4), Borgmassivet (n=3), and Huldreslottet (n=3; Figs. 2, 3). We primarily targeted quartz-bearing lithologies, although this proved difficult due to the widespread occurrence of mafic lithologies in this area (Groenewald et al., 1995). We principally sampled bedrock with glacial striations, and erratics resting firmly on bedrock, to avoid complications with post-depositional rotation and erosion (Fig. 4). All our samples were taken from wind-exposed sites, minimizing the risk of intermittent snow cover.

We recorded sample thickness, surface orientation, and topographic shielding for each sample in the field, and registered the position and elevation using a handheld GPS. We cross-checked registered site elevations against the Reference Elevation Model of Antarctica (REMA, 8 m spatial resolution and vertical errors typically <2 m, Howat et al., 2019), and find that GPS- and REMA-elevations differ by -12–33 m (mean 15±8 m). We use the GPS-derived elevation values for our age calculations, but the REMA-derived elevations to calculate the relative elevation of our samples above the surrounding ice sheet.

Owing to challenges with retrieving suitable samples from the often steep-sided nunataks, and difficulties in separating sufficient quartz for cosmogenic nuclide analysis, we struggled to establish robust multi-nuclide elevation profiles. However, we were able to analyse 3-5 samples from each site. For samples where we were able to retrieve quartz (n=28), we analysed ^{10}Be and ^{26}Al, while for a subset of the quartz-bearing samples we also analysed ^{36}Cl in feldspar separates (n=6) or whole rock (n=1). For non-quartz bearing samples, we analysed ^{36}Cl from whole rock (n=7).

Fig. 4. *Photographs of samples collected along the Penck Trough, illustrating different sample types:* ***a)*** *the bedrock-erratic pair SVE03 and SVE02,* ***b)*** *GRU03, this photo also illustrates our sampling method using a rock-drill, hammer and wedges,* ***c)*** *bedrock sample BOR01 collected from ventifacted bedrock,* ***d)*** *MID05 erratic resting on bedrock,* ***e)*** *VID04 by the person to the right, note that this boulder is resting on a larger slab within a slope deposit and we cannot exclude post-depositional movement for this sample, and* ***f)*** *KUL03 (marked by red arrow) resting on bedrock.*

3.3. Laboratory methods and nuclide measurements

Mineral separation and Be, Al, and Cl chemical preparation took place at PRIME Lab, Purdue University. Samples were crushed and quartz separated from the 250–500 μm fraction via froth flotation, magnetic separation, heavy liquid separation, and etching in dilute HF/HNO_3 for a minimum of 3 days (Kohl and Nishiizumi, 1992). Purity of the quartz was tested through inductively coupled plasma-optical emission spectrometry (ICP-OES) analysis, before splits of the pure quartz were taken for analysis of ^{10}Be and ^{26}Al. The feldspar-rich float fraction from the froth flotation step, or 250-500 μm whole rock in absence of feldspars, was leached three times in an ultrasonic bath in 5% nitric acid and used for ^{36}Cl analyses.

Be and Al chemistry followed standard procedures (e.g. Ochs and Ivy-Ochs, 1997). All samples, including the processing blank that followed each batch of 4–7 field samples, were spiked with ~270 μg in-house prepared ^{9}Be carrier and, if necessary, spiked with Al carrier (Acros Organics) up to a total Al content of at least 1 mg. Following digestion in concentrated HF, an aliquot was removed for total-Al determination on ICP-OES, before the sample was dried down in the presence of 1 mL H_2SO_4. Fe and Ti were precipitated and removed at pH ~14 followed by Be-Al precipitation at neutral pH. The samples were taken up in oxalic acid to complex Al (von Blanckenburg et al., 2004) prior to anion- and cation chromatography. Finally, the Al and Be hydroxides were re-precipitated, washed, calcinated in a propane flame and mixed with niobium powder before loading into stainless steel cathodes for Accelerator Mass Spectrometry (AMS) analysis. Total-Al aliquots were dried down thrice in the presence of aqua regia and re-dissolved in 5% HNO_3 prior to ICP-OES analysis. Total Al in processing blanks averaged 101±1.4% of the added spikes (n=5), while measurements of Be in the same aliquots returned 101±1.1% of Be spike values for blanks and field samples (n=36). These measurements strengthen the reliability of total Al determinations and the Be carrier concentration.

For ^{36}Cl measurements, approximately 30 g of acid-leached whole rock or feldspar separate were spiked with ~ 1 mg isotopically enriched chlorine ($^{35}Cl/^{37}Cl = 273$). Samples were dissolved in a HF/HNO_3 mixture in a warm water bath (60 °C). Chlorine was precipitated as AgCl and purified through $BaSO_4$ precipitation and ion exchange chromatography before recovery through a second AgCl precipitation. Bulk and target rock chemistry for ^{36}Cl samples was commercially analysed at Bureau Veritas Commodities, Vancouver, Canada, using X-ray fluorescence (XRF) for major elements and ICP-OES for trace elements.

AMS analyses of ^{10}Be, ^{26}Al, and ^{36}Cl were performed at the 8 MV tandem accelerator at PRIME Lab, normalizing $^{10}Be/^{9}Be$ ratios to 07KNSTD (Nishiizumi et al., 2007), $^{26}Al/^{27}Al$ ratios to KNSTD (Nishiizumi, 2004), and $^{36}Cl/Cl$ measurements to standards prepared from NIST reference material SRM 4943 (Sharma et al., 1990). Ratios of $^{35}Cl/^{37}Cl$ were determined in the AMS on Faraday cups before acceleration, and total Cl determined through isotope dilution assuming binary mixing between natural chloride of known $^{35}Cl/^{37}Cl$ and the ^{35}Cl enriched spike (Desilets et al., 2006). All samples were corrected for background contamination using the processing blank following each batch of field samples. Total process and carrier blanks were $38\pm17\times10^{3}$ ^{10}Be atoms (n=5), $61\pm45\times10^{3}$ ^{26}Al atoms (n=5), and $334 \pm 59\times10^{3}$ ^{36}Cl atoms (n=3), accounting for <1.3% (^{10}Be), <0.6% (^{26}Al), and <1.8% (^{36}Cl) of total atoms measured for most samples, but up to 2.7% (^{10}Be) for the youngest, Holocene erratic. Reported uncertainties on the ratios and carrier concentrations were propagated through to the final reported results (the internal error). Complete analytical data appear in the supplementary tables.

3.4. Apparent age calculations, multi-nuclide data interpretation, and terminology

Data used to compute the apparent exposure ages are shown in Supplementary Tables 1, 2 (^{10}Be and ^{26}Al), 3 and 4 (^{36}Cl), while a summary of apparent exposure ages for all nuclides and samples are shown in Table 1. Apparent exposure ages were calculated for all samples and nuclides using CRONUScalc (Marrero et al., 2016; http://cronus.cosmogenicnuclides.rocks/2.0/) with the LSDn scaling scheme, and assuming zero surface erosion, no inheritance, and continuous surface exposure. If all three of these assumptions are satisfied, apparent exposure ages reflect the true exposure age of a site, i.e. in this study the time since a site was last covered by the East Antarctic Ice Sheet. To assess whether these assumptions are valid, it is useful to compare apparent ages from multiple samples collected in close proximity, as well as ages derived from multiple nuclides with different half-lives from the same sample. If several nearby samples yield the same apparent exposure ages, or samples in an elevation transect show systematically decreasing ages towards lower elevation, this adds strength to the inference that an apparent age represents the true deglaciation age of that site. This inference is also strengthened if apparent ages derived from multiple nuclides within the same sample overlap within uncertainty. However, it is important to note that short periods of burial by non-erosive ice or other surface cover can only be distinguished if the half-lives and analytical precision of the measured nuclides allow it. In the discussion, we evaluate the apparent exposure ages using these criteria for each of our sample sites.

Each sample within our dataset has 1–3 nuclides analysed. In the following, we use the term *minimum apparent exposure age* for the youngest apparent exposure age derived from the shortest half-life nuclide measured for each sample (typically ^{36}Cl or ^{26}Al). We interpret this minimum apparent exposure age for each sample as the maximum length of the current ice-free period, i.e. the maximum time since last ice cover. This is only valid if a sample has experienced negligible post-glacial surface cover (of e.g. rock, sediment, or snow), and if erratics have experienced no post-depositional movement or rotation. Based on our strict sampling criteria (described in Sec. 3.2.), we estimate that these expectations are reasonable for most samples within this study. In the Discussion, we highlight samples where this may not be the case.

Table 1. Summary of apparent exposure ages for all samples ordered by site in increasing distance to the grounding line.

Site	Sample ID	Type	Elevation (m a.s.l.)	10Be age* (ka)	26Al age* (ka)	36Cl age* (ka)
Straumsnutane	STR01	bedrock (striated, q-vein)	751	138 +- 11 [2.6]	90 +- 10 [2.5]	
	STR03	bedrock (q-vein)	807			89 +- 11 [3.9]
	STR06	bedrock (q-vein)	797			158 +- 15 [3.6]
	STR07	bedrock (q-vein)	791			139 +- 8.6 [2.8]
Sverdrupfjella	SVE02	erratic	842	114 +- 9.5 [2.8]	99 +- 12 [3]	
	SVE03	bedrock	842	71.6 +- 5.9 [1.7]	41.7 +- 4.7 [1.2]	19.1 +- 2.4 [0.6]
	SVE04	erratic (boulder)	878	130 +- 11 [2.7]	96 +- 11 [2.5]	
	SVE05	erratic (boulder)	891	141 +- 12 [3]	111 +- 13 [3.2]	
	SVE06	bedrock	904	97.3 +- 8.2 [2.7]	56.9 +- 6.4 [1.8]	23.9 +- 2.8 [0.6]
Gråsteinen	GRO01	bedrock (striated, q-vein)	1083	61 +- 5 [1.1]	47.3 +- 5.3 [1.4]	
	GRO03	bedrock (striated, q-vein)	902	37.6 +- 3.1 [0.9]	30.3 +- 3.5 [1.2]	
	GRO04	bedrock (striated)	1000	39.6 +- 3.4 [1.4]	28.6 +- 3.3 [1]	
Grunehogna	GRU03	erratic (boulder)	1270	138 +- 11 [2.1]	120 +- 14 [2.5]	
	GRU05	erratic (boulder)	1274	40.1 +- 3.3 [1]	39.2 +- 4.6 [1.8]	
	GRU07	bedrock (striated)	1190	174 +- 16 [6.7]	147 +- 17 [4.8]	
	KUL03	erratic (cobble)	1353	11.8 +- 1 [0.3]	11.4 +- 1.3 [0.3]	
Viddalskollen	VID01	bedrock (striated)	1327	152 +- 13 [3.8]	90 +- 10 [2.7]	46 +- 14 [9.7]
	VID03	bedrock (striated)	1183	37.8 +- 3.9 [2.6]	32 +- 3.7 [1.4]	19.3 +- 9.6 [8.8]
	VID04	erratic (boulder)	1177	5.5 +- 0.5 [0.3]	5.1 +- 0.7 [0.3]	
	VID05	bedrock (striated)	1278			56 +- 15 [8.3]
	VID06	erratic (cobble)	1275	63.9 +- 5.4 [1.8]	57.3 +- 6.4 [1.7]	
Midbresrabben	MID01	bedrock (striated)	1631	327 +- 28 [5.4]	184 +- 22 [4.6]	74.8 +- 6.7 [1.7]
	MID02	bedrock (striated)	1661	399 +- 35 [6.5]	230 +- 28 [6.2]	107.8 +- 7.1 [1.9]
	MID03	erratic (cobble)	1629	100 +- 8.1 [1.6]	81.5 +- 9.2 [2.1]	
	MID05	erratic (cobble)	1563	2.8 +- 0.3 [0.3]	2.7 +- 0.3 [0.1]	
	MID05 (duplicate)			2.5 +- 0.3 [0.1]	2.7 +- 0.3 [0.1]	
Penck Trough Assemblage	HOG02	erratic (boulder)	1418	814 +- 84 [32]	760 +- 120 [31.2]	
	MOT01	bedrock (striated)	1621	48.7 +- 5.5 [4]	31 +- 4.6 [3.2]	16.1 +- 2.3 [0.4]
	TPK01	bedrock (striated)	1626			20.9 +- 1.6 [0.4]
	YST06	erratic (boulder)	1679	98.6 +- 8.1 [2]	93 +- 11 [2.6]	
Borgmassivet	BOR01	bedrock (ventificated)	2387	Saturated	2000 +- 1000 [230.6]	
	BOR02	erratic (boulder)	2144	170 +- 15 [6.5]	120 +- 14 [3.6]	
	BOR03	bedrock (striated)	2146	2170 +- 310 [64.1]	1450 +- 350 [77.2]	
Huldreslottet	HUD02	erratic (cobble)	2030			16.9 +- 2.8 [1.2]
	HUD06	erratic (cobble)	2089	56.5 +- 4.7 [1.3]	30.4 +- 3.4 [0.8]	
	HUD10	bedrock (striated)	1881			17.3 +- 2.3 [0.4]

*Ages calculated with CRONUS Earth web calculators v 2.0 (Marrero et al. 2016), the global calibration dataset (Borchers et al. 2016), and the LSDn ('Sa') spallation scaling scheme. For further details see Section 3 and Supplementary Tables 1-4. Age uncertainties are external [internal].

3.5. Elevation above present ice

To gauge the amount of ice-sheet thickening necessary to cover each of our sample sites, the elevation of these sites relative to the present ice-sheet surface must be established. This is not straightforward since the nunataks tend to obstruct the ice flow, leading to large gradients in ice-sheet elevation across each nunatak. We extracted at least two elevation metrics for each sample to complement the elevation above sea level.

First, we subtracted the minimum Bedmap surface elevation within a 100 km wide swath zone along the Penck Trough from each sample GPS elevation above sea level, in order to detrend the data for the overall ice-surface gradients along the transect (Figs. 2, 5). This elevation metric highlights how much each sample site protrudes above the ice stream, which in turn reflects how much the ice sheet would have to thicken in order to completely inundate the sampled nunataks. The metric emphasizes, for example, that Straumsnutane (our lowest elevation sample site with regard to sea level) is positioned among the sites highest above the ice stream surface (Fig. 5).

Second, we extracted the elevation of each sample above the regional ice sheet. This elevation metric was extracted from REMA (Howat et al., 2019). We manually identified the elevation of the samples above the elevation at a major break-in-slope between the ice sheet and the sampled nunataks (typically when surface slopes increase consistently to >2–3º), rather than at the bedrock-ice boundary visible in satellite imagery, because stagnant ice or snowfields often cover the lower slopes of nunataks. This metric reflects how much thicker the regional ice sheet would have to be to inundate our sample sites, which is less than the elevation above the trough, because the ice sheet slopes towards the trough.

Finally, for samples on nunataks with large ice-surface gradients, we manually extracted the sample elevation above local depressions in the ice surface surrounding that nunatak from REMA. This metric reflects how much thicker the ice sheet would have to be locally to cover our sample sites.

The latter two metrics highlight the maximum and minimum ice-sheet thickening required to cover our sample sites locally and highlights the uncertainty in assessing the “elevation above ice” as a metric of use for ice-sheet modellers. The most appropriate elevation metric probably depends on whether ice-sheet thickening occurred as a result of (i) increased precipitation on the nunataks, in which case the elevation above local ice may be more representative, or (ii) dynamic thickening of the ice sheet by an outwards migration of the grounding line and a contemporaneous slow-down of the ice flow, in which case the elevation above the regional ice sheet may more accurately represent the ice thickening necessary to cover the sample site. In the following, these metrics are referred to as elevations above local ice and the regional ice sheet, respectively. Elevation metrics for each sample are listed in Supplementary Table 5.

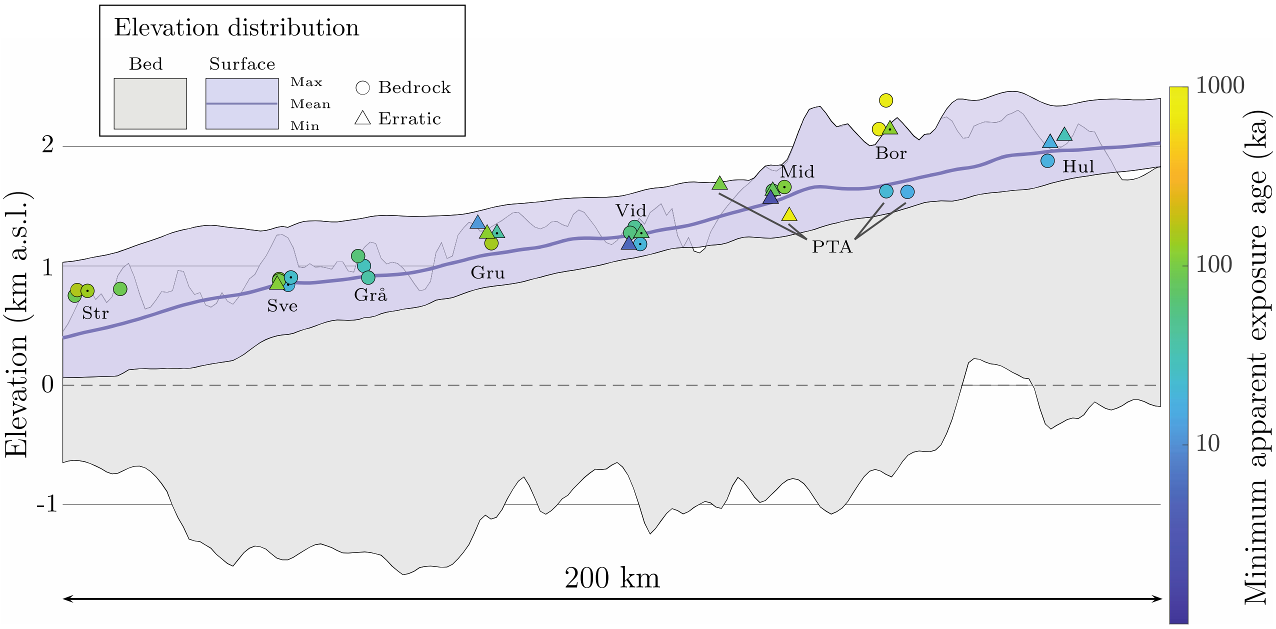

Fig. 5. *Topographic swath profile along the sample transect outlined in Fig. 2, showing maximum and minimum bed (grey band), and surface (purple band) elevations, mean surface elevation (purple line), and sample locations (circles and triangles) with minimum apparent exposure ages indicated by the fill colour on a logarithmic scale. Location of sample sites are indicated by the first three letters of the site names, except PTA = Penck Trough Assemblage. Samples with a black dot in the centre are shifted 2 km to the right, to improve visibility. Topographic data is sourced from Bedmap (Fretwell et al., 2013). Note that due to the low resolution of the Bedmap grid (1x1 km) some samples appear above the bedrock. The minimum surface elevation along this transect is subtracted from sample elevation above sea level to derive the 'elevation above ice stream' metric.*

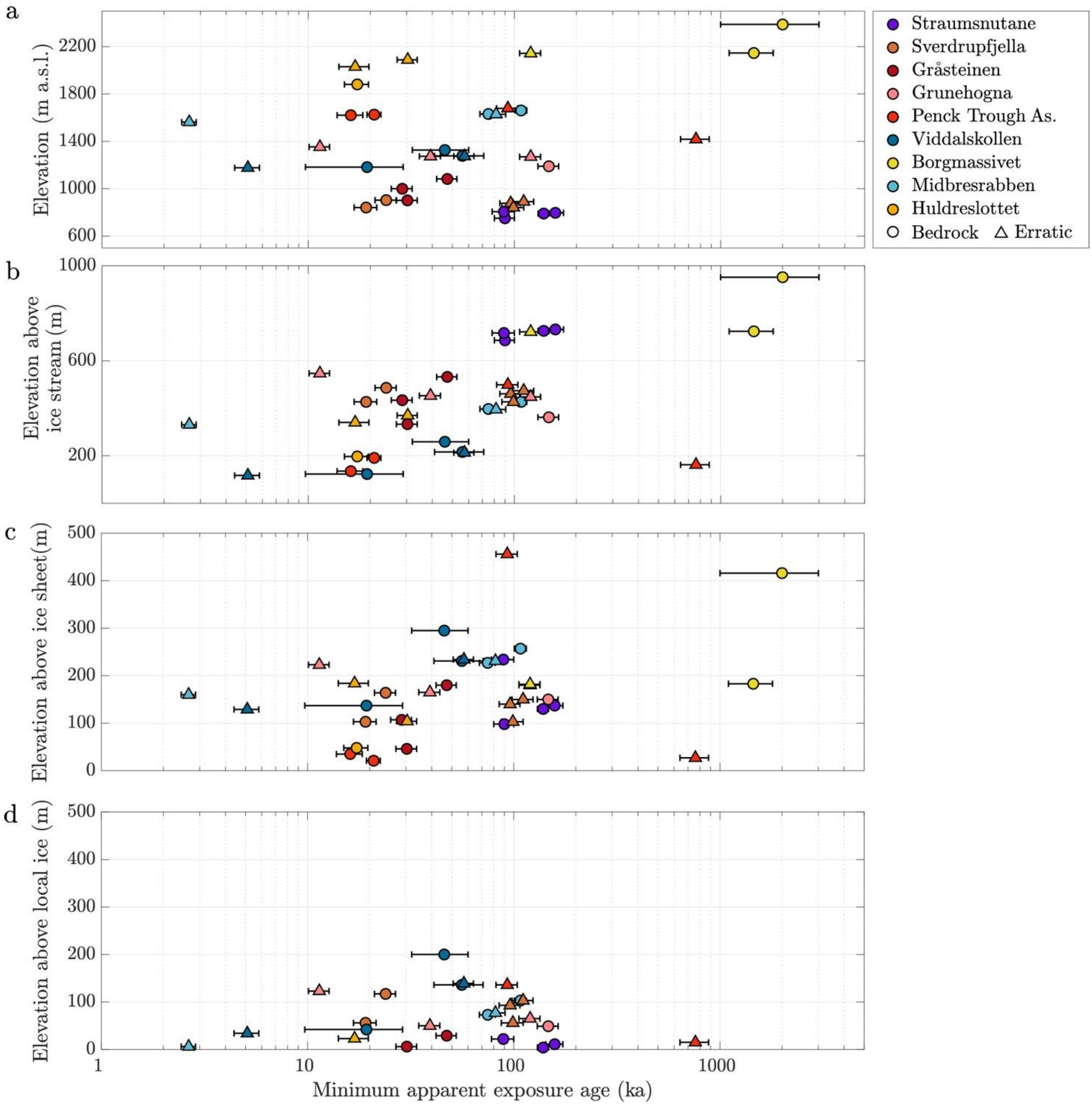

Fig. 6. *Minimum apparent exposure ages (note: logarithmic scale) as a function of elevation above* ***a)*** *present sea level,* ***b)*** *minimum ice surface elevation in the trough at the same distance from the grounding line as the sample,* ***c)*** *the present-day regional ice-sheet surface, and* ***d)*** *the local ice surface. Samples are coloured by sample site. Error bars show external uncertainties, which include cosmogenic nuclide production rate scaling uncertainties. Note that elevation above local ice surface was not determined for samples where local ice and the regional ice sheet is the same.*

4. Results

4.1. Data set overview and minimum ice thickening estimates

The samples within our dataset span elevations between 751 and 2387 m a.s.l. and have minimum apparent exposure ages between 2.6±0.2 [0.1] and 1450±350 [77] ka (± 1σ external [internal] uncertainty). More than 90% of the samples have ages younger than 160 ka, while ~25% have ages younger than the LGM (Fig. 6a; Table 1). Further, at least one sample from each of our sites is younger than 120 ka. This indicates that the ice sheet covered most of our sample sites within recent glacial cycles.

If minimum apparent exposure ages of our samples reflect the gradual thinning of the last glacial cover, a positive relation between elevation and age is expected. While the oldest minimum apparent exposure age is from the highest elevation site, there is no clear relationship between minimum apparent exposure ages and elevations of samples above sea level (Fig. 6a). Furthermore, surface elevations increase with distance inland from the grounding line, so there is also little overlap between the elevation of samples above present sea level between different sites along the coast-to-inland transect. In contrast, there is a clear, although scattered, positive relationship between minimum apparent exposure ages and sample elevations above the ice-stream surface (Fig. 6b), with the exception of a 750 ka old erratic from the Penck Trough Assemblage (HOG02). This pattern either indicates gradual ice thinning and/or decreased erosivity of the ice on peaks higher above the ice-stream surface, and thereby increased preservation of previously accumulated (inherited) nuclides. Excluding the Penck Trough Assemblage outlier, all samples <200 m above the ice-stream surface are <21 ka, while all samples <720 m above the ice-stream surface have minimum apparent exposure ages <150 ka. This indicates that, at face value, most sites below these elevation intervals above the current ice stream surface, were covered by ice during the last (or within the last two) glacial cycle(s), respectively.

The relationships between minimum apparent exposure ages and elevations above either the present-day regional ice sheet or local ice on the nunataks are scattered with a large range of minimum apparent exposure ages at the same elevation intervals (Figs. 6c, 6d). All samples <25 ka are located at elevations below 123/223 m above present-day local/regional ice sheet surfaces, while samples <160 ka are located below 200/295 m above present-day local/regional ice sheet surfaces with the exception of YST06 at 456 m above the regional ice sheet surface, which we discuss below. This demonstrates that ice almost certainly covered sites up to these elevations during or following the LGM and the two most recent glacial cycles, respectively.

It is important to note that all estimates are minimum estimates of ice thickening because i) the approach is limited by the height of the nunataks; i.e. our data can only record ice-sheet fluctuations up to the elevation of the highest sample, and ii) cosmogenic nuclide inheritance from previous exposure implies that true exposure ages of the samples are younger than the calculated apparent ages.

4.2. Coast to inland gradients in minimum ice-sheet thickening

Our samples form a series of elevation profiles along a transect from the grounding line to ~200 km inland along the Penck Trough (Fig. 2). This configuration allows us to evaluate the regional variations in minimum ice thickening from the present grounding line and inland in terms of minimum ice thickening during the LGM and the last glacial cycle.

At Straumsnutane near the present-day grounding line, none of the four bedrock samples yield ages younger than the LGM (minimum apparent ages ~90–160 ka, Fig. 7, Table 1) so we cannot ascertain whether the LGM ice sheet covered Straumsnutane nunataks. Yet, our results indicate that at least two of the samples were covered within the last glacial cycle, among these the sample highest above the ice (STR03, 22/234 m above local/regional ice). Because our samples from Straumsnutane are situated higher above the ice stream than most of our other samples (Fig. 5), the absence of ages younger than LGM could be either due to an absence of ice coverage during the LGM or lack of erosion by a thin, non-erosive, ice sheet and thus more preservation of inherited nuclides in the bedrock.

Further inland, on the eastern side of Jutulstraumen, our highest bedrock sample (SVE06) from Sverdrupfjella (40 km from the grounding line) has a minimum apparent exposure age of 24.0±2.8 [0.6] indicating that the nunatak probably was covered by the LGM ice sheet up to at least this level (117/164 m above local/regional ice). SVE06 was collected at the upper edge of a scattered till deposit, but whether this boundary represents the maximum extent of the LGM ice at this location remains unresolved, since we did not obtain good samples at higher elevation. The three erratics found at lower elevations at Sverdrupfjella all contain inherited nuclides and have minimum apparent exposure ages ranging from 96 ka to 111 ka, whereas the lower bedrock sample (SVE03, Fig. 4a) at 56/103 m above the local/regional ice sheet has a minimum apparent exposure age of 19.0±2.4 [0.6] ka.

Our three bedrock samples at Gråsteinen, ~55 km from the grounding line have minimum apparent exposure ages ~30–50 ka, indicating ice cover during the last glacial cycle, though not necessarily during the LGM. However, considering the relatively young ages, and that sample sites at similar elevations above the ice sheet on both sides of Jutulstraumen (Sverdrupfjella and Grunehogna) were covered during the LGM (Fig. 7), it seems most plausible that our samples at Gråsteinen were also covered, but that bedrock erosion was insufficient to remove all the nuclides from previous exposure. This is further supported by ^{10}Be-^{26}Al inventories indicating complex exposure (Fig. 8). We infer that the LGM ice sheet did cover these samples, as indicated by the red dashed lines in Fig. 7.

Young apparent exposure ages from the highest erratic sample (KUL03; Fig. 4f) from the Grunehogna nunataks, ~75 km inland, indicate deposition by the LGM ice sheet, and that ice retreated from this site at 11.6 ± 0.8 [0.2] ka. The erratic is located ~120 m above local ice to the east and ~220 m above the regional ice sheet to the NW, making this sample an important indicator of ice-sheet thickening during or following the LGM. The three other Grunehogna samples are from other nunataks within the same area, are collected at lower elevations above the ice sheet, (49-65/150–180 m above local/regional ice), are older (39–147 ka), and most likely contain some inheritance.

At Viddalskollen, a nunatak protruding through the ice sheet ~105 km inland from the grounding line in the middle of the Penck Trough, the two lower samples (34–42/129–137 m above local/regional ice) indicate LGM ice cover (5–19 ka), while the three higher samples (136–200/231-295 m above local/regional ice) indicate ice cover during the last glacial cycle (46–57 ka) or more recently. Similarly, at Midbresrabben, ~130 km inland, the lower erratic sample (MID05, Fig. 4d, 6/160 m above local/regional ice) indicates ice cover during or following the LGM (2.6±0.1 [0.1] ka), whereas the three higher samples (73–103/227–257 m above local/regional ice) indicate ice cover during the last glacial cycle (75–108 ka) or more recently.

Between Viddalskollen and Midbresrabben, a single erratic sample (YST06) from Ystenut nunatak (Penck Trough Assemblage) indicates ice cover within the last glacial cycle (93 ± 11 [2.6] ka). Because this sample is located 456 m above the ice sheet, it indicates a much thicker ice sheet than the surrounding samples (Fig. 7). However, the sample is collected on a ridge, only slightly protruding an ice-covered slope towards the ice sheet. A subtle thickening of the ice sheet may be enough to decrease the angle of this slope and thereby cover this sample. We thus suggest a lower minimum ice-sheet thickening during the last glacial period, schematically indicated by the blue dashed line on Fig. 7a.

At Borgmassivet, ~150 km inland from the grounding line, two bedrock samples from the Penck Trough Assemblage indicate LGM ice cover (16–21 ka, 21–35 m above the adjacent Penck Trough Ice Stream), while two bedrock samples ~200–400 m above the ice sheet indicate near-continuous exposure for millions of years (Fig. 7). The lower of these bedrock samples is, however, found next to a much younger erratic (120 ± 14.0 [3.6] ka) indicating ice coverage within recent glacial cycles. The young minimum apparent exposure age of this erratic, dating from the end of the last interglacial period, and a complex history inferred from multi-nuclide inventories (Fig. 8) indicate that the erratic could easily have been deposited within the last glacial cycle. We return to a discussion of the significance of the old bedrock samples from Borgmassivet for EAIS glaciation history in Section 4.4.

Finally, the samples from Huldreslottet, ~180 km inland of the current grounding line, indicate ice coverage during or following the LGM up to elevations 23–48/48–184 m above the present local/regional ice sheet surface. A bedrock and an erratic sampled at the bottom (HUD10, 1881 m a.s.l.) and top (HUD02, 2030 m a.s.l.) of a steep slope on this nunatak (Fig. 3), both yield apparent exposure ages of ~17 ka (Table 1). A single erratic on a separate nunatak ~3 km further from the ice stream (HUD06) yields a minimum apparent exposure age of 30.4 ± 3.4 [0.8] ka, but the multi-nuclide (^{26}Al, ^{10}Be) inventories indicate a high degree of inheritance (Fig. 8).

Regional minimum ice-sheet thickening estimates can be constructed for LGM and last glacial cycle configurations by plotting the elevations above present local/regional ice sheet surface elevations against the sample distance from the grounding line along the trough (Fig. 7). This shows that minimum ice-sheet thickening for the LGM (exposure ages younger than 25 ka) ranges from 175/220 m above the local/regional ice sheet at distances ~40–75 km from the grounding line, to 50/190 m above the local/regional ice sheet 100–200 km inland. When using the elevations above the regional ice sheet, ice thickening is rather uniform along the transect (Fig. 7a), whereas for elevations above the local ice surface, the minimum thickening decreases between 75 and 100 km distance from the grounding line (Fig. 7b), and remains below 100 m. Correspondingly, the minimum thickening for the last glacial cycle (exposure ages younger than 110 ka), varies from 175/234 m above the local/regional ice sheet at distances up to 75 km from the grounding line, to 200/300 m above the local/regional ice sheet (excluding YST06 at 456 m) 100–200 km inland, with the highest minimum thickening ~100–140 km inland.

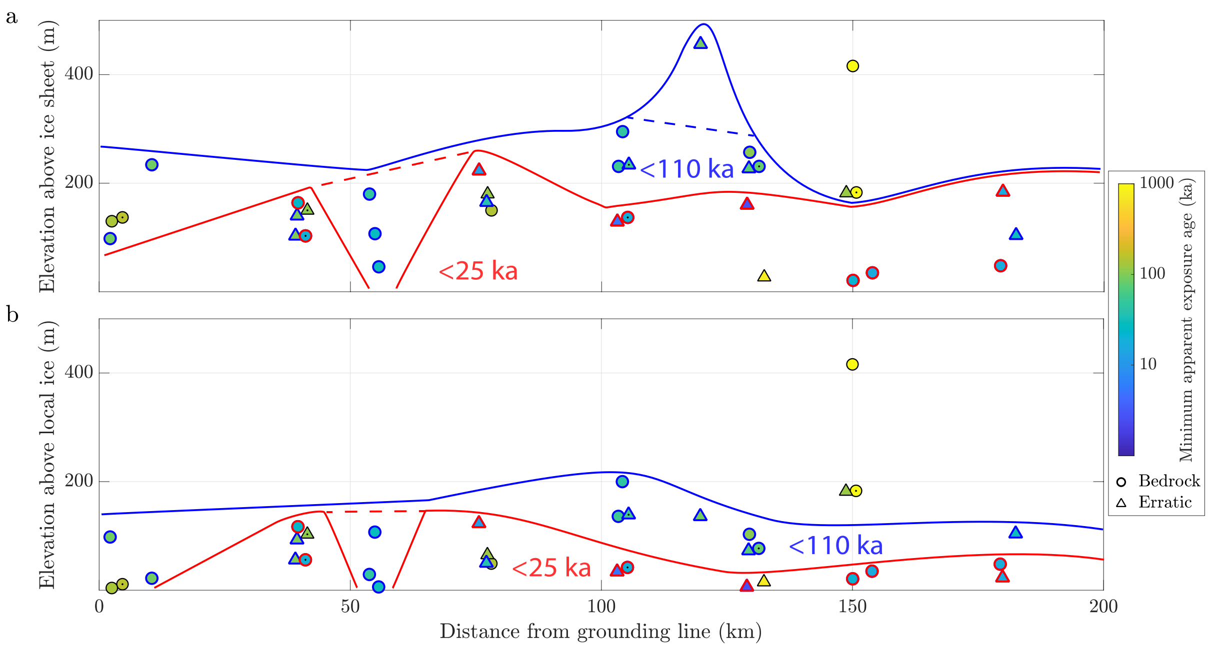

Fig. 7. *Sample distance from grounding line as a function of elevation above* ***a)*** *the regional ice-sheet surface, and* ***b)*** *the local ice surface. Samples are coloured by minimum apparent exposure ages, note the logarithmic scale. Samples highlighted with a red outline are younger than 25 ka (~LGM), while samples with a blue outline are younger than 110 ka (~last glacial cycle), and the red and blue lines sketch the minimum thickening of the EAIS in this region necessary to cover these samples within the last 25 and 110 ka respectively. Note that these are minimum estimates of thickening. Dashed sections indicate smoother solutions discussed in Section 4.2.*

4.3. Timing of last ice thinning

While minimum apparent exposure ages provide maximum estimates for the timing of last ice retreat, more data are needed to evaluate whether these ages represent the actual time of last ice cover. Unfortunately, samples in our dataset are too spatially scattered to allow for statistical outlier detection within groups of samples from the same site and elevation (Balco, 2011; Blomdin et al., 2016; Jones et al., 2019), or along elevation profiles (Small et al., 2019). Instead we use multiple nuclides with different half-lives measured in the same sample to evaluate this question. Concordance between apparent ages derived from different nuclides, and/or nuclide inventories falling on the simple exposure island in the two-isotope plot (Fig. 8), indicate a simple exposure history, which increases our confidence that the apparent ages reflect the last ice cover, while diverging results indicate complex histories characterised by one or more periods of burial beneath non-erosive ice or recent exhumation from beneath till or rock (Knudsen and Egholm, 2018).

Whereas most of our samples indicate complex exposure (Fig. 8, Table 1), three erratic samples provide ^{10}Be and ^{26}Al data that are indistinguishable from a simple exposure scenario and have exposure ages younger than LGM. Of these, MID05 (6/160 m above local/regional ice surface elevations) provides a weighted average age (duplicate measurement of both ^{10}Be and ^{26}Al, using inverse squares of external [internal] uncertainty as weights) of 2.6±0.2 [0.1] ka, VID04 (34/129 m above local/regional ice surface elevations) provides an age of 5.3±0.4 [0.2] ka (weighted average of ^{10}Be and ^{26}Al), and KUL03 (123/223 m above local/regional ice surface elevations) yields 11.6±0.8 [0.2] ka (weighted average of ^{10}Be and ^{26}Al). These samples stem from different nunataks situated on each side (Grunehogna and Midbresrabben) and in the middle (Viddalskollen) of the Penck Trough Ice Stream, on the western side of Jutulstraumen (Fig. 2). Unfortunately, we cannot exclude post-depositional movement of VID04 (Fig. 4e), as this sample was collected from the top of a large (1.2 x 0.8 x 0.7 m) boulder within a slope deposit, albeit in a stable position according to the field assessment. In contrast, MID05 (Fig. 4d) and KUL03 both were found on bedrock in stable positions and furthermore were small enough (longest axes <15 cm) to allow for processing of the entire cobbles. Three additional erratic samples yield apparently simple exposure ages, but the ages predate LGM. Of these, HOG02 (15/27 m above local/regional ice surface elevations) yields 796±69 ka, YST06 (136/456 m above local/regional ice surface elevations) yields 96.6±6.5 ka, and GRU05 (50/165 m above local/regional ice surface elevations) returns an age of 39.8±2.7 ka (weighted average ages of ^{10}Be and ^{26}Al using inverse squares of external uncertainties as weights). Because HOG02 is situated immediately adjacent to the Penck Trough Ice Stream, ~50 km up-stream of its junction with Jutulstraumen, we infer deposition of this sample during recent glaciations with a high degree of inheritance, although limited burial (Fig. 8). The minimum apparent exposure age of YST06 indicate deposition within the last glacial cycle, possibly during the LGM. GRU05 was collected 80 m lower than KUL03 which indicates glacial cover until ~11 ka, but it was collected from a separate nunatak 3 km away, so we cannot exclude ice-free conditions during the LGM.

Seven additional samples provide ^{36}Cl minimum apparent exposure ages (24–16 ka) close to or younger than LGM (Table 1). Four of these samples (SVE03, SVE06, VID03, MOT01) are known to have complex exposure histories based on results obtained from ^{26}Al and ^{10}Be from the same samples (Fig. 8). Their minimum apparent exposure ages are thus affected by inheritance. For the three additional samples, we only have ^{36}Cl measurements on whole rock (no quartz could be obtained), and it cannot be assessed whether these ages have simple or complex exposure histories. Two of these samples come from Huldreslottet and have apparent ages overlapping within uncertainty (HUD02: 16.9±2.8 [1.2] ka and HUD10: 17.3±2.3 [0.4] ka), which requires both samples (one erratic, one striated bedrock) to either represent a simple exposure history or a similar level of ^{36}Cl inheritance. The last of these samples, TPK01, immediately adjacent to the Penck Trough Ice Stream (bedrock, 21 m above local ice surface) returns an apparent exposure age of

20.9±1.6 [0.4] ka. The remaining samples in the dataset have apparent ages exceeding the LGM, and do not aid us in constraining the timing of last ice thinning. In a forthcoming manuscript, we explore the long-term exposure- and erosion history of the region through inverse modelling of multi-nuclide inventories of complex bedrock samples (Andersen et al., in prep).

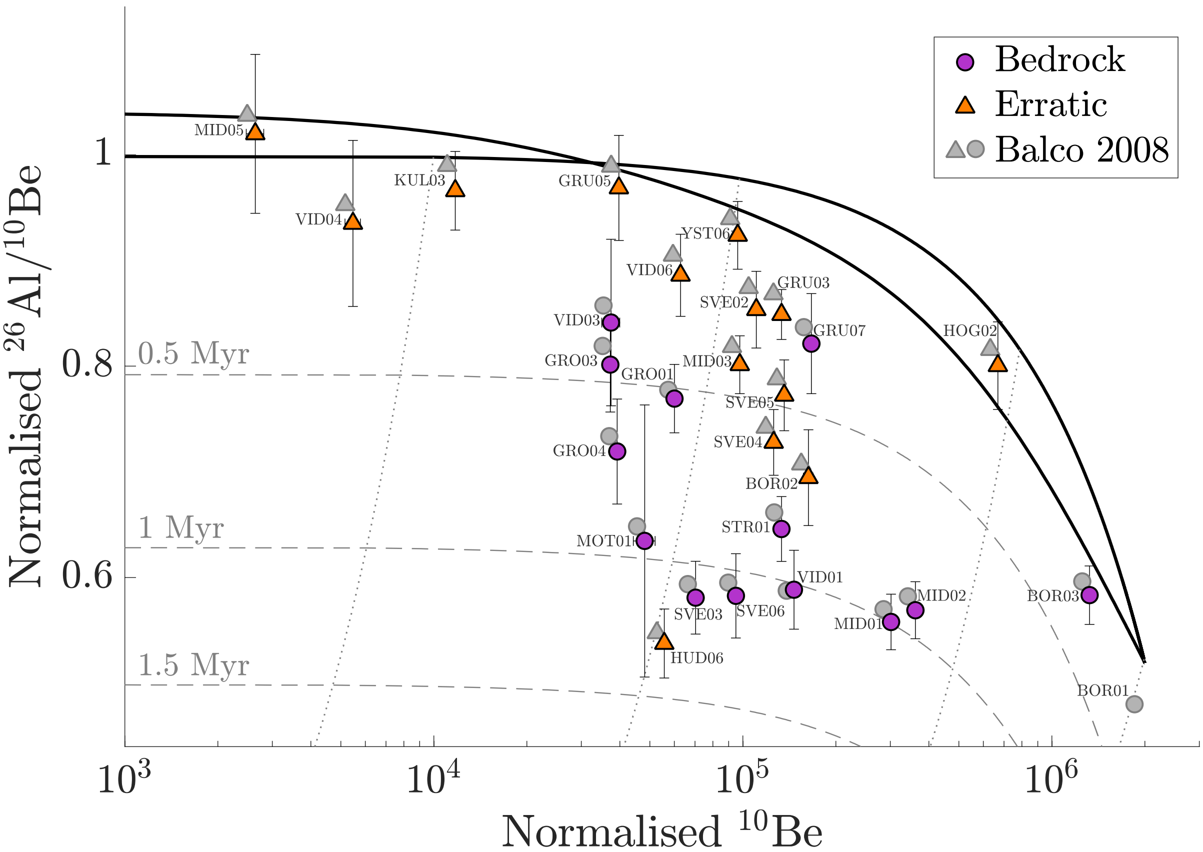

Fig. 8. *Two-isotope diagram of* ^{26}*Al/*^{10}*Be ratios versus* ^{10}*Be abundances normalised by the site production rates derived from CRONUScalc by Marrero et al. (2016; coloured markers) and the calculators formerly known as the CRONUS-Earth calculators by Balco et al. (2008; grey markers, error bars omitted for figure simplicity). Note that BOR01 is saturated with regard to CRONUScalc derived production rates and thus is not displayed. The solid black lines represent the steady state erosion island, whereas the dotted lines trace the decay-controlled burial paths below this island, and the dashed lines indicate the duration of burial (0.5, 1.0, and 1.5 Myr) within a simple two-stage exposure-burial scenario. Samples overlapping the steady erosion island indicate simple exposure histories with limited burial beneath non-erosive ice or other surface covers. Samples falling beneath this island indicate complex exposure-burial histories.*

4.4. Maximum LGM ice thickness

Whereas the majority of samples within our dataset yield relatively young (<160 ka) apparent exposure ages, the two bedrock samples from Borgmassivet provide the oldest apparent exposure ages within our dataset (Table 1). Both samples are collected from bedrock ridges that flank the local ice cap on the Borgmassivet nunatak (Fig. 3a).

The highest of these samples (BOR01: 2387 m a.s.l., 416 m above the regional ice sheet), a bedrock surface with a ventifacted appearance (Fig. 4c), provides a minimum apparent exposure age of 2.0±1.0 [0.23] Ma (^{26}Al) and a ^{10}Be concentration above saturation given the LSDn scaling scheme in CRONUScalc (Marrero et al., 2016), whereas ages calculated by applying the same scaling scheme, but using the online calculator formerly known as the CRONUS-Earth online calculator (Balco et al., 2008, http://hess.ess.washington.edu) version 3, yield apparent ages of 2.1±0.63 [0.16] Ma (^{26}Al) and 5.2±1.5 [0.48] Ma (^{10}Be). The high ^{10}Be and ^{26}Al inventories and the ventifacted appearance of BOR01 are indicative of long exposure duration with low erosion rates (Fig. 8). In fact, it may have been continuously exposed since the Pliocene, with steady erosion rates around 0.15±0.03 [0.009] m Ma^{-1} (^{10}Be) to 0.30±0.08 [0.02] m Ma^{-1} (^{26}Al) (calculated using Balco et al., 2008)). However, the two-isotope plot (Fig. 8) indicates that this sample experienced some burial. Given uncertainties in the ^{26}Al/^{10}Be production ratio or possibly the ^{26}Al half-life (Balco, 2019), we are not certain whether this is real. Owing to production and measurement uncertainties, and the long half-lives of the measured nuclides, we cannot determine whether this sample was ever covered by glacial ice. Assuming current production rate estimates, zero erosion, and a single burial event, the maximum burial duration this sample has experienced is ~150–200 kyr if burial is recent, or ~500 kyr if burial is distributed through the last 1 Ma (Balco et al., 2014). Burial prior to 1 Ma would reduce these estimates.

High-elevation cosmogenic nuclide bedrock apparent exposure ages from eastern Dronning Maud Land also indicate near-continuous exposure with similarly-low erosion rates (Matsuoka et al., 2006; Altmaier et al., 2010; Suganuma et al., 2014; Strub et al., 2015; Yamane et al., 2015). As pointed out by Altmaier et al. (2010), the low erosion rates in Dronning Maud Land point to the longevity of the present polar, hyper-arid conditions. Partial or full burial adds to the total time these samples have spent near the surface, and thus the longevity of hyper-arid conditions.

The lower (striated) bedrock sample from Borgmassivet (BOR03: 2146 m a.s.l., 183 m above the regional ice sheet) provides an apparent ^{10}Be age of 2.2±0.3 Ma, and ^{10}Be and ^{26}Al inventories nearly consistent with continuous exposure and steady erosion (Fig. 8; 0.30±0.04 [0.01] m Ma^{-1} (^{10}Be) and 0.40±0.09 [0.02] m Ma^{-1} (^{26}Al)). However, a nearby erratic boulder (BOR02: 2144 m a.s.l.) displays complex, but much younger, apparent exposure ages (Fig. 8; ^{10}Be: 170 ± 15.0 [6.5] ka, ^{26}Al: 120 ± 14.0 [3.6] ka), indicative of more recent (<~120 ka), burial by non-erosive or weakly-erosive ice.

5. Discussion

5.1. Indications of a thicker post-LGM ice sheet

A number of samples within our dataset provide constraints on post-LGM ice-sheet fluctuations within the study area. Although scattered, these samples provide targets for ice-sheet models intended to capture first order trends in EAIS fluctuations in Dronning Maud Land.

Only two samples (MID05, KUL03) from two different nunataks provide data that most likely record the timing of last glacial thinning (~11.6–2.6 ka), while we cannot exclude that a third young sample with nuclide inventories indicating simple exposure (VID04; 5.3±0.4 [0.2] ka) was impacted by slope processes. Although these samples point to thinning within the Holocene, no thinning rate estimates can be calculated, and we also note the lack of statistical robustness from not having multiple samples in close proximity yielding similar results. However, the conclusion that the EAIS was thicker during or since the LGM in this region is supported by seven additional samples with minimum apparent exposure ages within or younger than the LGM. Since these samples either have multi-nuclide ages indicating a complex exposure-burial history, or only have one nuclide (^{36}Cl) measured, the ages represent Holocene exposure in addition to an unknown component of inheritance, and are thus maximum estimates of the timing of last ice cover. Two of these samples from the same nunatak at Huldreslottet (HUD02 and HUD10, 180 km from the grounding line), have apparent ^{36}Cl ages overlapping within uncertainty, indicating ice-sheet thinning in this area since or after ~17 ka.

The spatial distribution of samples with minimum apparent ages younger than the LGM provides some constraints on the minimum ice surface thickening during or following the LGM. The minimum ice thickening above the present-day ice sheet is thus ~100/200 m, depending on whether we use the elevation above local ice or above the regional ice sheet. It is ambiguous which elevation is more representative of the actual ice-sheet thickening in this region, as the bedrock and ice-sheet topography are heavily entwined. Ice-surface changes are thus likely to depend on the evolving ice-sheet dynamics and the distribution of precipitation, and ice modelling simulations are needed to answer this question.

Sixteen samples yield minimum apparent ages older than the LGM (>25 ka), but within the last glacial cycle (<110 ka). These samples were possibly deposited or covered by the ice sheet at the LGM, in which case they contain inherited nuclides, but were certainly covered within the last glacial period (<110 ka). The minimum thickening of the ice-sheet surface within the last glacial period based on these samples is ~150/300 m above the local/regional ice sheet, with a grounding-line to inland trend showing little variation, although the highest minimum thickness estimates are found ~100–140 km inland (Fig. 7).

Although no robust thinning estimates could be established, our results are consistent with radiocarbon ages derived from Mumiyo deposits from Snow Petrel nesting sites 30–60 km NW of SANAE IV research base, near the present grounding line (Fig. 2). These data indicate ice-free conditions at elevations ~1-100 m above the ice sheet during the latter half of the Holocene (<8.0 cal ka BP, Steele and Hiller, 1997).

5.2. Maximum ice thickness during recent glacial cycles

The maximum ice-sheet thickening during recent glacial periods cannot be robustly resolved with our dataset. In fact, only our highest bedrock sample from Borgmassivet (BOR01: 2387 m a.s.l.) is indicative of long-term near-continuous exposure, while a bedrock-erratic pair at a few hundred meters lower elevation indicate short-lived burial by weakly erosive ice (BOR02 and BOR03: ~2145 m a.s.l.) within the last ~120 ka (assuming no erosion or post-depositional rotation of the erratic). It thus appears that the Borgmassivet near-summit ridge at 2387 m a.s.l. remained mostly ice-free throughout at least the Pleistocene and possibly much longer, although we cannot ascertain whether it was ice-free throughout the last glacial cycle, and non-erosive burial of a duration up to ~500 ka within the last million years remains possible. In contrast, the EAIS or a local ice cap covered our lower Borgmassivet site for short periods of time within recent global glacial cycles.

Whereas BOR01 indicates near-continuous exposure at high elevation 150 km from the grounding line, no maximum constraint on ice thickness could be established along the remainder of the transect. The only further constraint our dataset offers, is that most of our bedrock samples, and particularly those near the present grounding line (Straumsnutane, Sverdrupfjella), contain inherited nuclides indicating limited erosion, and therefore cold-based conditions of recent overriding ice sheets. The ice thickness theoretically necessary for basal ice to reach the pressure melting point thus sets an upper limit to recent ice thickness above these nunataks (Näslund et al. 2000). Basal temperatures are determined by the geothermal heat flow, the snow accumulation rate, surface temperatures, and the ice thickness. It is estimated that the majority of the ice sheet in Dronning Maud Land is currently cold-based and substantial ice thickening would be required to raise basal ice temperature to the pressure melting point (Näslund et al. 2000).

5.3. Gradients in LGM ice-sheet thickening along the Dronning Maud Land coast

In eastern Dronning Maud Land, the ice surface during the LGM was likely <100 m above the present-day ice-sheet surface 65–135 km from the present-day grounding line in the Sør Rondane Mountains (Matsuoka et al., 2006; Suganuma et al., 2014; Yamane et al., 2015), and <50 m above the present surface 80–160 km from the grounding line in the Wohlthat Massif (Altmaier et al., 2010; Strub et al., 2015). In contrast, our results point to at least ~200 m thickening above the present-day regional ice sheet 40-180 km inland along the Penck Trough (Fig. 7a). Our results thus indicate a thicker LGM ice sheet along the Penck Trough and the Jutulstraumen ice stream, compared to published data from eastern Dronning Maud Land. Furthermore, ice thickening seems to extend further inland than in eastern Dronning Maud Land. Our results from the Penck Trough are in line with undated records from Vestfjella mountains in the westernmost part of Dronning Maud Land (Fig. 1), which are suggested to imply more than 700 m thicker ice during the LGM near the present-day grounding line, although with diminishing magnitudes inland (Lintinen 1996; Lintinen and Nenonen, 1997). Furthermore, new *in-situ* ^{14}C records from the Shackleton Range indicate 350–650 m thicker ice along the Slessor glacier, near the present grounding line (Nichols et al., 2019). Together, these results point to a gradient in ice surface thickening during the LGM along the coast of Dronning Maud Land, with increasing ice thickening towards the Weddell Sea. However, since several studies from eastern Dronning Maud Land only report a single nuclide (^{10}Be), it remains possible that the inferred limited LGM ice thickening in this region is a result of prevalent nuclide inheritance in bedrock and erratics. Further analyses with *in-situ* ^{14}C from all sites would help answering this question, as well as illuminate the rates and timing of post-LGM ice-sheet thinning.

In contrast to eastern Dronning Maud Land sites, the sites investigated in this study straddle the two largest ice streams in the area, the Jutulstraumen and Penck Trough ice streams which merge within our study area (Fig. 2). The location of both ice streams is structurally controlled, and they occupy deep troughs with a maximum depth of more than 1.6 km below sea level. Due to this topographic setting it seems likely that these ice streams remained active conduits for ice flow throughout most of the glaciated history of this margin. Additionally, the level of the ice surface within the ice streams probably acts as a base level for ice sheet thickness within adjacent areas. We suggest that the thickening of the ice sheet in the trough region during the last glacial cycle, which is demonstrated by our results, was coeval with grounding line progradation and controlled ice thickening within adjacent areas. We envisage the Jutulstraumen and Penck Trough ice streams as active conduits that were thicker, rather than the thickening being the result of the ice streams 'switching off' during cold periods. However, we note that the increased distance to the ocean, smaller vertical gradients of the ice surface, and a colder ice sheet, probably lead to a general reduction of ice velocities within our study area both within and outside current ice streams areas.

The escarpment plays an important role for the configuration of the ice sheet in Dronning Maud Land, as evidenced by changes in surface temperatures, snow accumulation, and elevation of the ice sheet across this boundary (see Background section). Since ice-core records indicate a thinner ice sheet on the polar plateau above the escarpment during global glacial periods, and because results from cosmogenic nuclide studies across coastal ice sheet sectors indicate ice-sheet thickening (although of a more limited extent in eastern Dronning Maud Land), this topographic step in the ice surface was likely less prominent during the LGM. The ice discharge across this escarpment could thus have been lower during the LGM than at present owing to the combination of lower inland precipitation and lower ice surface gradients. Our reconstruction of ice surface changes below the escarpment, combined with future high-resolution ice-sheet models, will enable the investigation of the role of the escarpment on ice-sheet dynamics across glacial cycles.

6. Conclusions

Nunataks protruding through the East Antarctic Ice Sheet (EAIS) in western Dronning Maud Land preserve records of past ice-surface fluctuations that can be constrained with cosmogenic nuclide exposure dating methods. However, low erosion rates below the ice sheet lead to widespread occurrence of inherited nuclides in exposed rock, posing a methodological challenge.

In this study, we investigated the exposure history of nunataks fringing the Penck Trough and the lower reaches of the Jutulstraumen Ice Stream using a multi-nuclide approach (^{10}Be, ^{26}Al, ^{36}Cl). Although many of our samples contain an inherited signal, indicating multiple cycles of exposure and burial beneath predominantly cold-based ice, minimum estimates of LGM and last glacial cycle thickening of the EAIS in this region were established. These estimates show that the ice sheet was at least 100-200 m thicker than present within the last 25 ka, and at least 150–300 m thicker within the last glacial cycle. The large range in minimum elevation estimates is a result of the highly topographically-controlled ice-sheet surface, complicating the determination of sample elevation above the present ice sheet. Our samples form a transect from the grounding line and ~200 km inland along the Penck Trough, demonstrating that ice-sheet thickening during the last glacial cycle had a regional character, although possibly with a decreasing magnitude of ice thickening inland.

Although a few samples from this study indicate ice-sheet thinning ~35–120 m towards the present ice sheet surface during the Holocene, questions remain regarding the exact timing of ice-sheet thinning within our study area that we hope to resolve with future *in-situ* ^{14}C measurements.

The maximum thickening of the ice sheet during the last glacial cycle is not well constrained by our results, as only our single highest sample (2387 m a.s.l., 150 km inland from the grounding line) indicates near-continuous exposure since at least the Pliocene. However, the measurement uncertainties and long half-lives of the measured nuclides (^{10}Be and ^{26}Al) mean that we are unable to exclude ice cover during the last glacial period even for this sample.

Ice streams act as base levels for ice flow in the region. We suggest that progradation of the grounding line is the most likely explanation for ice thickening within the ice streams and adjacent areas. Compared to published results from eastern Dronning Maud Land, our data indicate more extensive ice thickening during the LGM and last glacial cycle, with ice thickening propagating further inland along the Penck Trough. Ice thickening of several hundred meters or more is consistent with undated records from Vestfjella mountains further west in Dronning Maud Land, and our results are also consistent with an east-west gradient in LGM ice thickening along the Dronning Maud Land coast towards the Weddell Sea.

Acknowledgements

This material is based upon work supported by Stockholm University (APS), Norwegian Polar Institute/NARE under Grant "MAGIC-DML" (OF), the US National Science Foundation under Grant No. PLR-1542930 (JMH & NL) and EAR-1560658 (MWC), Swedish Research Council under Grant No. 2016-04422 (JMH & APS), the German Research Foundation (DFG), Priority Programme 1158 "Antarctic Research" under Grant No. 365737614 (IR), and the German Aerospace Centre (DLR) for TerraSAR-X/TanDEM-X data under grant "DEM_GLAC1773" (OF).

We thank the Swedish Polar Research Secretariat for logistical support, UNAVCO for providing the dGPS, and PGC for provision of satellite data used for navigation in the field. JLA was supported by a Carlsberg Foundation Fellowship.

Author contributions

The study was conceived by APS, JMH, IR, DF, OF, NFG, and NAL. Sample material was collected by JCN, RB, SES, DF, and JMH. Sample preparation and analysis undertaken by JLA, AJK, and JCN. JLA analysed the data, and wrote the manuscript with contributions from all authors.

References

Altmaier, M., Herpers, U., Delisle, G., Merchel, S., & Ott, U. (2010). Glaciation history of Queen Maud Land (Antarctica) reconstructed from in-situ produced cosmogenic 10Be, 26Al and 21Ne. *Polar Science*, *4*(1), 42-61.

Andersen, J.L., Newall, J.C.H, Sams, S., Koester, A., Blomdin, R., Fabel, D., Glasser, N., Lifton, N., Caffee, M. Fredin, O., Harbor, J., Stroeven, A.P.: A thick East Antarctic ice sheet margin dominated western Dronning Maud Land in the Pleistocene. In preparation.

Anderson, J. B., Shipp, S. S., Lowe, A. L., Wellner, J. S., & Mosola, A. B. (2002). The Antarctic Ice Sheet during the Last Glacial Maximum and its subsequent retreat history: a review. *Quaternary Science Reviews*, *21*(1-3), 49-70.

Arthern, R. J., Winebrenner, D. P., & Vaughan, D. G. (2006). Antarctic snow accumulation mapped using polarization of 4.3- cm wavelength microwave emission. *Journal of Geophysical Research: Atmospheres*, *111*(D6).

Balco, G., Stone, J. O., Lifton, N. A., & Dunai, T. J. (2008). A complete and easily accessible means of calculating surface exposure ages or erosion rates from 10Be and 26Al measurements. *Quaternary geochronology*, *3*(3), 174-195.

Balco, G. (2011). Contributions and unrealized potential contributions of cosmogenic-nuclide exposure dating to glacier chronology, 1990–2010. *Quaternary Science Reviews*, *30*(1-2), 3-27.

Balco, G., Stone, J. O., Sliwinski, M. G., & Todd, C. (2014). Features of the glacial history of the Transantarctic Mountains inferred from cosmogenic 26 Al, 10 Be and 21 Ne concentrations in bedrock surfaces. *Antarctic Science*, *26*(6), 708-723.

Balco, G. (2019, February 5). Stone (2000) revisited [Blog Post]. Retrieved from https://cosmognosis.wordpress.com/2019/02/05/stone-2000-revisited/

Bentley, M. J., Cofaigh, C. O., Anderson, J. B., Conway, H., Davies, B., Graham, A. G., ... & Mackintosh, A. (2014). A community-based geological reconstruction of Antarctic Ice Sheet deglaciation since the Last Glacial Maximum. *Quaternary Science Reviews*, *100*, 1-9.

Blomdin, R., A.P. Stroeven, J.M. Harbor, N.A. Lifton, J. Heyman, N. Gribenski, D.A. Petrakov, M.W. Caffee, M.N. Ivanov, C. Hättestrand, I. Rogozhina & R. Usubaliev 2016. Evaluating the timing of former glacier expansions in the Tian Shan: a key step towards robust spatial correlations. *Quaternary Science Reviews,* 153, 78-96.

Borchers, B., Marrero, S., Balco, G., Caffee, M., Goehring, B., Lifton, N., ... & Stone, J. (2016). Geological calibration of spallation production rates in the CRONUS-Earth project. *Quaternary Geochronology*, *31*, 188-198.

Briner, J.P., Lifton, N.A., Miller, G.H., Refsnider, K., Anderson, R., Finkel, R., 2014. Using in situ cosmogenic 10Be, 14C, and 26Al to decipher the history of polythermal ice sheets on Baffin Island, Arctic Canada. Quaternary Geochronology 19, 4–13. doi:10.1016/j.quageo.2012.11.005

Chmeleff, J., von Blanckenburg, F., Kossert, K., & Jakob, D. (2010). Determination of the 10Be half-life by multicollector ICP-MS and liquid scintillation counting. *Nuclear Instruments and Methods in Physics Research Section B: Beam Interactions with Materials and Atoms*, *268*(2), 192-199.

Comiso, J. C. (2000). Variability and trends in Antarctic surface temperatures from in situ and satellite infrared measurements. *Journal of Climate*, *13*(10), 1674-1696.

DeConto, R. M., & Pollard, D. (2003). Rapid Cenozoic glaciation of Antarctica induced by declining atmospheric CO_2. *Nature*, *421*(6920), 245-249.

DeConto, R. M., & Pollard, D. (2016). Contribution of Antarctica to past and future sea-level rise. *Nature*, *531*(7596), 591-597.

Desilets, D., Zreda, M., Almasi, P. F., & Elmore, D. (2006). Determination of cosmogenic 36Cl in rocks by isotope dilution: innovations, validation and error propagation. *Chemical Geology*, *233*(3-4), 185-195.

Elverhøi, A. (1981). Evidence for a late Wisconsin glaciation of the Weddell Sea. *Nature*, *293*(5834), 641-642.

Fretwell, P., Pritchard, H. D., Vaughan, D. G., Bamber, J. L., Barrand, N. E., Bell, R., ... & Catania, G. A. (2013). Bedmap2: improved ice bed, surface and thickness datasets for Antarctica. *The Cryosphere*, *7*(1), 375-393.

Goldstein, G. (1966). Partial half-life for β-decay of 36Cl. *Journal of Inorganic and Nuclear Chemistry*, *28*(4), 937-939.

Gore, D. B., Rhodes, E. J., Augustinus, P. C., Leishman, M. R., Colhoun, E. A., & Rees-Jones, J. (2001). Bunger Hills, East Antarctica: ice free at the last glacial maximum. *Geology*, *29*(12), 1103-1106.

Gosse, J. C., & Phillips, F. M. (2001). Terrestrial in situ cosmogenic nuclides: theory and application. *Quaternary Science Reviews*, *20*(14), 1475-1560.

Groenewald, P. B., Moyes, A. B., Grantham, G. H., & Krynauw, J. R. (1995). East Antarctic crustal evolution: geological constraints and modelling in western Dronning Maud Land. *Precambrian Research*, *75*(3-4), 231-250.

Hodgson, D. A., Noon, P. E., Vyverman, W., Bryant, C. L., Gore, D. B., Appleby, P., ... & Ellis-Evans, J. C. (2001). Were the Larsemann Hills ice-free through the last glacial maximum? *Antarctic Science*, *13*(4), 440-454.

Hogg, A. G., Hua, Q., Blackwell, P. G., Niu, M., Buck, C. E., Guilderson, T. P., ... & Turney, C. S. (2013). SHCal13 Southern Hemisphere calibration, 0–50,000 years cal BP. *Radiocarbon*, *55*(4), 1889-1903.

Holden, N.E., 1990. Total half-lives for selected nuclides, Pure Appl. Chem. 62 941–958.

Howat, I. M., Porter, C., Smith, B. E., Noh, M.-J., and Morin, P. (2019): The Reference Elevation Model of Antarctica, *The Cryosphere*, 13, 665-674, *https://doi.org/10.5194/tc-13-665-2019, 2019*.

Hättestrand, C., & Johansen, N. (2005). Supraglacial moraines in Scharffenbergbotnen, Heimefrontfjella, Dronning Maud Land, Antarctica–significance for reconstructing former blue ice areas. *Antarctic Science*, *17*(2), 225-236.

Jones, R. S., Small, D., Cahill, N., Bentley, M. J., & Whitehouse, P. L. (2019). iceTEA: Tools for plotting and analysing cosmogenic-nuclide surface-exposure data from former ice margins. *Quaternary Geochronology*, *51*, 72-86.

Kohl, C. P., & Nishiizumi, K. (1992). Chemical isolation of quartz for measurement of in-situ-produced cosmogenic nuclides. *Geochimica et Cosmochimica Acta*, *56*(9), 3583-3587.

Korschinek, G., Bergmaier, A., Faestermann, T., Gerstmann, U. C., Knie, K., Rugel, G., ... & Kossert, K. (2010). A new value for the half-life of 10Be by heavy-ion elastic recoil detection and liquid scintillation counting. *Nuclear Instruments and Methods in Physics Research Section B: Beam Interactions with Materials and Atoms*, *268*(2), 187-191.

Knudsen, M. F., & Egholm, D. L. (2018). Constraining Quaternary ice covers and erosion rates using cosmogenic 26Al/10Be nuclide concentrations. *Quaternary Science Reviews*, *181*, 65-75.

Lenaerts, J. T., van Meijgaard, E., van den Broeke, M. R., Ligtenberg, S. R., Horwath, M., & Isaksson, E. (2013). Recent snowfall anomalies in Dronning Maud Land, East Antarctica, in a historical and future climate perspective. *Geophysical Research Letters*, *40*(11), 2684-2688.

Lintinen, P. (1996). Evidence for the former existence of a thicker ice sheet on the Vestfjella nunataks in western Dronning Maud Land, Antarctica. *Bulletin-Geological Society of Finland*, *68*, 85-98.

Lintinen, P., & Nenonen, J. (1997). Glacial history of the Vestfjella and Heimefrontfjella nunatak ranges in western Dronning Maud Land, Antarctica. *The Antarctic Region: Geological Evolution and Processes*, 845-852.

Livingstone, S. J., Cofaigh, C. Ó., Stokes, C. R., Hillenbrand, C. D., Vieli, A., & Jamieson, S. S. (2012). Antarctic palaeo-ice streams. *Earth-Science Reviews*, *111*(1-2), 90-128.

Mackintosh, A. N., Verleyen, E., O'Brien, P. E., White, D. A., Jones, R. S., McKay, R., ... & Miura, H. (2014). Retreat history of the East Antarctic Ice Sheet since the last glacial maximum. *Quaternary Science Reviews*, *100*, 10-30.

Marrero, S. M., Phillips, F. M., Borchers, B., Lifton, N., Aumer, R., & Balco, G. (2016). Cosmogenic nuclide systematics and the CRONUScalc program. *Quaternary Geochronology*, *31*, 160-187.

Matsuoka, N., Thomachot, C. E., Oguchi, C. T., Hatta, T., Abe, M., & Matsuzaki, H. (2006). Quaternary bedrock erosion and landscape evolution in the Sør Rondane Mountains, East Antarctica: Reevaluating rates and processes. *Geomorphology*, *81*(3-4), 408-420.

Matsuoka, K., Skoglund, A., & Roth, G. (2018). Quantarctica 3 [Data set]. Norwegian Polar Institute. https://doi.org/10.21334/npolar.2018.8516e961

Medley, B., McConnell, J. R., Neumann, T. A., Reijmer, C. H., Chellman, N., Sigl, M., & Kipfstuhl, S. (2018). Temperature and snowfall in western Queen Maud Land increasing faster than climate model projections. *Geophysical Research Letters*, *45*(3), 1472-1480.

Mengel, M., Nauels, A., Rogelj, J., & Schleussner, C. F. (2018). Committed sea-level rise under the Paris Agreement and the legacy of delayed mitigation action. *Nature communications*, *9*(1), 601.

Miura, H., Moriwaki, K., Maemoku, H., & Hirakawa, K. (1998). Fluctuations of the East Antarctic ice-sheet margin since the last glaciation from the stratigraphy of raised beach deposits along the Soya Coast. *Annals of Glaciology*, *27*, 297-301.

Näslund, J. O., Fastook, J. L., & Holmlund, P. (2000). Numerical modelling of the ice sheet in western Dronning Maud Land, East Antarctica: impacts of present, past and future climates. *Journal of Glaciology*, *46*(152), 54-66.

Nichols, K. A., Goehring, B. M., Balco, G., Johnson, J., Hein, A. S., & Todd, C. (2019). New Last Glacial Maximum ice thickness constraints for the Weddell Sea Embayment, Antarctica. *The Cryosphere*, *13*(11), 2935-2951.

Nishiizumi, K. (2004). Preparation of 26Al AMS standards. *Nuclear Instruments and Methods in Physics Research Section B: Beam Interactions with Materials and Atoms*, *223*, 388-392.

Nishiizumi, K., Imamura, M., Caffee, M. W., Southon, J. R., Finkel, R. C., & McAninch, J. (2007). Absolute calibration of 10Be AMS standards. *Nuclear Instruments and Methods in Physics Research Section B: Beam Interactions with Materials and Atoms*, *258*(2), 403-413.

Ochs, M., Ivy-Ochs, S., 1997. The chemical behavior of Be, Al, Fe, Ca and Mg during AMS target preparation from terrestrial silicates modeled with chemical speciation calculations. Nuclear Instruments and Methods in Physics Research Section B 123, 235–240. doi:10.1016/S0168-583X(96)00680-5

Parrenin, F., Dreyfus, G., Durand, G., Fujita, S., Gagliardini, O., Gillet, F., Jouzel, J., Kawamura, K., Lhomme, N., Masson-Delmotte, V., Ritz, C., Schwander, J., Shoji, H., Uemura, R., Watanabe, O., and Yoshida, N. (2007): 1-D-ice flow modelling at EPICA Dome C and Dome Fuji, East Antarctica. *Clim. Past,* 3 (243–259), https://doi.org/10.5194/cp-3-243-2007

Rignot, E., Mouginot, J., & Scheuchl, B. (2011). Ice flow of the Antarctic ice sheet. *Science*, *333*(6048), 1427-1430.

Rignot, E., Mouginot, J., & Scheuchl, B. (2017). MEaSUREs InSAR-based Antarctica ice velocity map, version 2. *National Snow & Ice Data Center*: https://nsidc.org/data/NSIDC-0484/versions/2

Riva, R. E., Gunter, B. C., Urban, T. J., Vermeersen, B. L., Lindenbergh, R. C., Helsen, M. M., ... & Schutz, B. E. (2009). Glacial isostatic adjustment over Antarctica from combined ICESat and GRACE satellite data. *Earth and Planetary Science Letters*, *288*(3-4), 516-523.

Schröder, L., Horwath, M., Dietrich, R., Helm, V., van Den Broeke, M. R., & Ligtenberg, S. R. (2019). Four decades of Antarctic surface elevation changes from multi-mission satellite altimetry. *The Cryosphere*, *13*(2), 427-449.

Sharma, P., Kubik, P. W., Fehn, U., Gove, H. E., Nishiizumi, K., & Elmore, D. (1990). Development of 36Cl standards for AMS. *Nuclear Instruments and Methods in Physics Research Section B: Beam Interactions with Materials and Atoms*, *52*(3-4), 410-415.

Small, D., Bentley, M. J., Jones, R. S., Pittard, M. L., & Whitehouse, P. L. (2019). Antarctic ice sheet palaeo-thinning rates from vertical transects of cosmogenic exposure ages. *Quaternary Science Reviews*, *206*, 65-80

Smedsrud, L. H., Jenkins, A., Holland, D. M., & Nøst, O. A. (2006). Modeling ocean processes below Fimbulisen, Antarctica. *Journal of Geophysical Research: Oceans*, *111*(C1).

Steele, W. K., & Hiller, A. (1997). Radiocarbon dates of snow petrel (Pagodroma nivea) nest sites in central Dronning Maud Land, Antarctica. *Polar Record*, *33*(184), 29-38.

Stroeven A.P., Fabel D., Hättestrand C., Harbor J., (2002). A relict landscape in the centre of Fennoscandian glaciation: cosmogenic radionuclide evidence of tors preserved through multiple glacial cycles *Geomorphology* 44, 145–154.

Stroeven, A. P., Hättestrand, C., Kleman, J., Heyman, J., Fabel, D., Fredin, O., ... & Caffee, M. W. (2016). Deglaciation of fennoscandia. *Quaternary Science Reviews*, *147*, 91-121.

Strub, E., Wiesel, H., Delisle, G., Binnie, S. A., Liermann, A., Dunai, T. J., ... & Coenen, H. H. (2015). Glaciation history of Queen Maud Land (Antarctica)–New exposure data from nunataks. *Nuclear Instruments and Methods in Physics Research Section B: Beam Interactions with Materials and Atoms*, *361*, 599-603.

Stuiver, M., & Reimer, P. J. (1993). Extended 14 C data base and revised CALIB 3.0 14 C age calibration program. *Radiocarbon*, *35*(1), 215-230.

Suganuma, Y., Miura, H., Zondervan, A., & Okuno, J. I. (2014). East Antarctic deglaciation and the link to global cooling during the Quaternary: evidence from glacial geomorphology and 10Be surface exposure dating of the Sør Rondane Mountains, Dronning Maud Land. *Quaternary Science Reviews*, *97*, 102-120.

Thomas, I. D., King, M. A., Bentley, M. J., Whitehouse, P. L., Penna, N. T., Williams, S. D., ... & Hindmarsh, R. C. (2011). Widespread low rates of Antarctic glacial isostatic adjustment revealed by GPS observations. *Geophysical Research Letters*, *38*(22).

van de Berg, W. J., van den Broeke, M. R., Reijmer, C. H., & van Meijgaard, E. (2006). Reassessment of the Antarctic surface mass balance using calibrated output of a regional atmospheric climate model. *Journal of Geophysical Research: Atmospheres*, *111*(D11).

Velicogna, I., & Wahr, J. (2006). Measurements of time-variable gravity show mass loss in Antarctica. *science*, *311*(5768), 1754-1756.

Velicogna, I., & Wahr, J. (2013). Time- variable gravity observations of ice sheet mass balance: Precision and limitations of the GRACE satellite data. *Geophysical Research Letters*, *40*(12), 3055-3063.

von Blanckenburg, F., Hewawasam, T., & Kubik, P. W. (2004). Cosmogenic nuclide evidence for low weathering and denudation in the wet, tropical highlands of Sri Lanka. *Journal of Geophysical Research: Earth Surface*, *109*(F3).

Yamane, M., Yokoyama, Y., Abe-Ouchi, A., Obrochta, S., Saito, F., Moriwaki, K., & Matsuzaki, H. (2015). Exposure age and ice-sheet model constraints on Pliocene East Antarctic ice sheet dynamics. *Nature Communications*, *6*, 7016.